Effects of Combustor Exit Profiles on Vane Aerodynamic Loading and Heat Transfer in a High Pressure Turbine

M. D. Barringer

K. A. Thole

Department of Mechanical and Nuclear Engineering,
The Pennsylvania State University,
University Park, PA 16802

M. D. Polanka

Air Force Research Laboratory,
Turbines Branch,
WPAFB, OH 45433

The flow and thermal fields exiting gas turbine combustors dictate the overall performance of the downstream turbine. The goal of this work was to investigate the effects of engine representative combustor exit profiles on high pressure turbine vane aerodynamics and heat transfer. The various profiles were produced using a nonreacting turbine inlet profile generator in the Turbine Research Facility (TRF) located at the Air Force Research Laboratory (AFRL). This paper reports how the pressure loading and heat transfer along the vane surface was affected by different turbine inlet pressure and temperature profiles at different span locations. The results indicate that the inlet total pressure profiles affected the aerodynamic loading by as much as 10%. The results also reveal that the combination of different total pressure and total temperature profiles significantly affected the vane heat transfer relative to a baseline test with uniform inlet total pressure and total temperature. Near the inner diameter endwall, the baseline heat transfer was reduced 30–40% over the majority of the vane surface. Near the outer dimeter endwall, it was found that certain inlet profiles could increase the baseline heat transfer by 10–20%, while other profiles resulted in a decrease in the baseline heat transfer by 25–35%. This study also shows the importance of knowing an accurate prediction of the local flow driving temperature when determining vane surface heat transfer.
[DOI: 10.1115/1.2950051]

Introduction

The desire to continuously improve the performance and working life of aircraft gas turbine engines has led to the need for more advanced engine hardware that is capable of surviving in very intense flow and thermal environments. Improvements in engine performance can come in the form of increasing thrust production while increasing the working life of the individual engine components. Increasing the thrust can be accomplished by increasing the gas working temperature of the turbine section. As a result of the push for higher temperatures, the gas temperatures exiting combustors of modern engines are well above the melting point of the metal alloy engine components. The durability and maintainability of these engine parts are therefore primary concerns of gas turbine engine designers. Of particular interest is the interface between the combustor and turbine sections where the high pressure turbine vanes are subjected to the very harsh, highly turbulent, and nonuniform flow fields exiting the combustor.

The complexity of the combustor exit flow stems from the intense flow interactions that take place within the central chamber of the combustor. This chamber consists primarily of inlet flow swirlers, fuel nozzles, inner diameter (ID) and outer diameter (OD) annular liners, and an overall exit contraction. The annular liners typically contain primary holes and dilution holes that inject large amounts of air into the central chamber to first help stabilize combustion and then to dilute the combustion products to reduce the overall gas temperature to a level acceptable for the turbine hardware. The liners also contain film cooling holes and slots that inject cooling air along the liner walls to form a protective layer of insulating air that shields the metal from the relatively hot combustion gas. As the individual flow streams travel down the length of the chamber, they combine and interact with one another, resulting in a highly nonuniform flow structure at the combustor exit. The spatial variations in temperature impose nonuniform heat transfer on the high pressure turbine vanes and blades that can result in local melting and cracking of the metal and can thus permanently damage strategic cooling features. The elevated turbulence levels act to intensify this heat transfer by increasing local convection heat transfer coefficients to the vane surface. The spatial variations in the pressure at the combustor exit can result in nonuniform aerodynamic loading that can increase local thermal-mechanical stresses.

Turbine engine designers have been forced to prepare for the worst case when designing the high pressure vanes and blades without knowing exactly how the combustor exit profiles affect the hardware. For example, some designers currently use a radial pressure profile consistent with a standard turbulent boundary layer as the inlet condition to the turbine while designing their vanes and blades. However, more realistic combustor exit flows can result in turbine inlet profiles and secondary flow development that is significantly different from what has been used as a design condition. A better understanding of how the combustor exit flow alters the flow development and heat transfer within the downstream turbine is needed. This understanding can be accomplished by studying how different combustor exit profile shapes impact the downstream turbine components.

The primary research objective of this paper was to study the effects of several radial pressure and temperature profiles on high pressure turbine vane aerodynamic loading and heat transfer. The profiles analyzed in this study were produced by the nonreacting inlet profile generator (combustor simulator) that is located in the Turbine Research Facility (TRF) at the Air Force Research Laboratory (AFRL) and described in Barringer et al. [1].

Contributed by the International Gas Turbine Division of ASME for publication in the JOURNAL OF TURBOMACHINERY. Manuscript received October 10, 2006; final manuscript received December 3, 2007; published online January 23, 2009. Review conducted by Je-Chin Han. Paper presented at the ASME Turbo Expo 2006: Land, Sea and Air (GT2006), Barcelona, Spain, May 8—11, 2006.

Relevant Past Studies

Several studies have been performed to analyze and model the flow and thermal fields within aircraft engine combustors and turbines. Few studies, however, have focused on how the combustor exit environment affects the performance of the downstream turbine. Rather, most studies have been isolated to analyzing either the combustor section or the turbine section alone. Studying the interaction of the combustor exit flow with the turbine is crucial to fully understanding how the vanes and blades are influenced by different realistic inlet conditions. This understanding will help turbine designers improve their own research and development work. The following is a review of some past and recent studies that have focused on the interface between the combustor and turbine sections.

The effect of different inlet radial temperature profiles on the aerodynamic performance of a transonic turbine stage was investigated by Cattafesta [2] using the MIT blow-down Turbine facility. Tests with similar corrected flow conditions but with different temperature profiles changed the overall turbine efficiency by 2%. Shang et al. [3] conducted similar tests using a full turbine stage in the same facility to study the influence of inlet temperature distortion on rotor blade heat transfer. It was found that changing the stage inlet turbulence intensity from 0.5–8% did not influence the rotor blade surface heat flux. Radial thermal distortions near midspan, with peak temperatures 10% larger than the mean, resulted in significant augmentation of local blade heat transfer along the pressure side (PS) in the tip and hub regions. This radial temperature distortion resulted in Nusselt numbers 10% higher than those measured with uniform conditions within the tip region and 50% higher within the hub region. The Nusselt numbers measured at midspan were nearly the same with and without the radial temperature distortion.

Chana et al. [4] conducted research using a nonuniform inlet temperature generator at the QinetiQ transient turbine research facility. Cold gas was injected upstream of the turbine section at the hub and tip to shape the temperature profile in the radial direction and through turbulence rods inserted into the main flow to shape it in the circumferential direction. Results showed that vane heat transfer was affected by the presence of the nonuniform temperature profile on the suction surface of the turbine nozzle guide vanes. Povey et al. [5] conducted similar research in the same QinetiQ facility and outlined a thorough review of recent and past studies involving high pressure experimental facilities used to simulate and study combustor exit flows, some of which are mentioned in this literature review. An important finding from their study was the significant augmentation to the vane heat transfer when comparing uniform turbine inlet temperature profiles to the vane heat transfer measured when the inlet temperature profile possessed maximum nonuniform conditions of T/T_{av} near 10%. Their study also discussed a method to determine the vane surface and endwall heat transfer driving temperature based on knowledge of the Nusselt number with uniform inlet temperature and inlet temperature distortion. Their method assumes that the heat transfer coefficient is unchanged with and without the inlet temperature distortion.

Krishnamoorthy et al. [6] investigated the effect of combustor exit turbulence on a downstream turbine vane cascade. Their results indicated that the effect of high turbulence at the combustor exit was to reduce the cooling effectiveness on the vane by 10%. It was also shown that the effect of temperature nonuniformities at the combustor exit was to reduce the overall cooling effectiveness on the vane by as much as 21%. Van Fossen and Bunker [7] studied heat transfer augmentation in the stagnation region of a flat plate with an elliptical leading edge. The test article was located downstream of an arc segment of a dual-annular combustor. The swirl driven combustor flow produced turbulence intensities up to approximately 32% with length scales near 1.3 cm. Augmentation of heat transfer was found to be very significant in the range of 34–59%. No effect of circumferential position with respect to the upstream swirlers was found.

There have been few investigations into the effects of inlet profiles on endwall secondary flow development. These are important as they distribute the temperature field and generate turbulence. As shown in the literature, the secondary flows present within turbine vane passages originate at the leading edge vane–endwall junction. The horseshoe vortex that forms at this leading edge junction splits into two vortices, one of which progresses to the vane PS and one to the suction side (SS). The PS leg of the horseshoe vortex travels down the endwall along the upstream portion of the PS of the vane during which it merges with and becomes the passage vortex. This passage vortex crosses over the channel along the endwall toward the SS of the adjacent vane. It then travels down the endwall along the latter portion of the SS of this adjacent vane. The SS leg of the horseshoe vortex is much smaller in size relative to the PS vortex and passage vortex. This SS leg travels along the endwall corner of the vane suction surface until it is overcome by the passage vortex.

Studies by Hermanson and Thole [8] have shown that the total pressure field is a driving force in the development of secondary flows and heat transfer present in turbine vane passages. They also reported that a counter-rotating vortex can exist, in addition to the passage vortex, within the vane passage that can drive fluid away from the endwall and toward midspan. This counter-rotating vortex was found for an inlet total pressure profile containing a positive inflection point in the spanwise direction near the endwall.

Colban et al. [9] studied the effects of varying FC flow through the liner and exit junction slot in a large scale, low speed combustor simulator on the adiabatic effectiveness, and secondary flow development within a downstream turbine cascade. Results showed that varying the coolant injection through the liner led to different total pressure profiles entering the downstream turbine section. Measurements showed that the coolant exiting the liner and slot accumulated along the SS of the vane and endwall and that increasing the FC flow through the liner did not result in a continual increase in adiabatic effectiveness values.

Their study also documented the vane passage secondary flow vectors for different vane inlet total pressure profiles and confirmed the presence of a counter-rotating vortex located above the passage vortex when the vane inlet pressure profile contains a slight forward facing peak near the endwall. This is illustrated in Fig. 1, which shows secondary flow vectors within the vane passage (at approximately $X/C=0.35$) for two different vane inlet pressure profiles. The type A profiles, shown in Fig. 1(*a*), possess the typical shape of a turbulent boundary layer with lower total pressure near the endwall relative to midspan, and the type B profiles, shown in Fig. 1(*b*), contain a forward facing inflection point. This inflection point is caused by the injection of high flow out of the cooling liner holes resulting in a high total pressure region near the endwall at $Z/\mathrm{Sp}=0.1$ relative to midspan. The size and location are dependent on the amount of coolant ejected.

To summarize, the current research to date suggests that certain heat transfer trends within the turbine section are due to nonuniform inlet temperature and pressure conditions. Studies have reported significant augmentation of heat transfer along the SS of the vanes and the PS of the blades in both the hub and tip regions with insignificant changes noted near midspan. Also, the literature contains few experimental data that document total pressure profiles at the combustor exit. The goal of this work is not only to verify some of the important trends found in the literature but, more importantly, to enhance the understanding of the impact of more realistic turbine inlet profiles. In addition to representative combustor exit temperature profiles, realistic pressure profiles are also studied to quantify the effects of both on high pressure turbine vane heat transfer and aerodynamics. This study will provide some new insight to further enhance future turbine development.

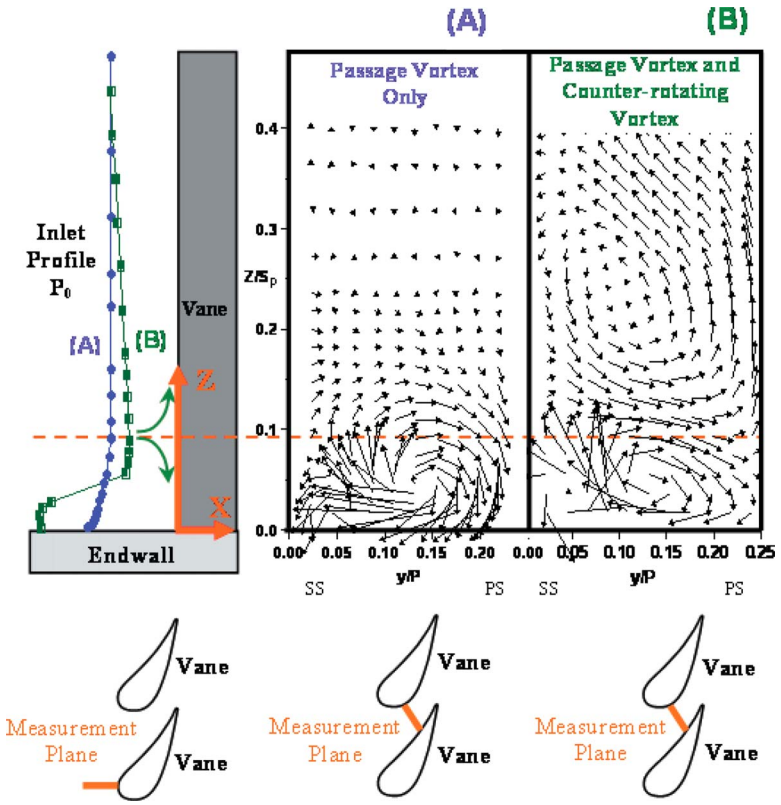

Fig. 1 Velocity contours within the vane passage ($X/C=0.35$) from Colban et al. [9] showing secondary flow vectors and their corresponding vane inlet total pressure profiles for (A) a turbulent boundary layer and (B) a forward facing inflection point near the endwall

Experimental Facility and Instrumentation

The experimental facility used in this study is the TRF at the AFRL at Wright Patterson Air Force Base in Dayton, Ohio. The TRF, documented in Haldeman et al. [10], is a short duration blow-down test facility that can match engine Reynolds number, Mach number, pressure ratio, gas to metal temperature ratio, corrected speed, and corrected mass flow. The facility is shown in Fig. 2, and it consisted primarily of a large supply tank, a turbine test section, and two large vacuum tanks. The turbine test section was a true scale, fully annular, half turbine stage, consisting of high pressure vanes.

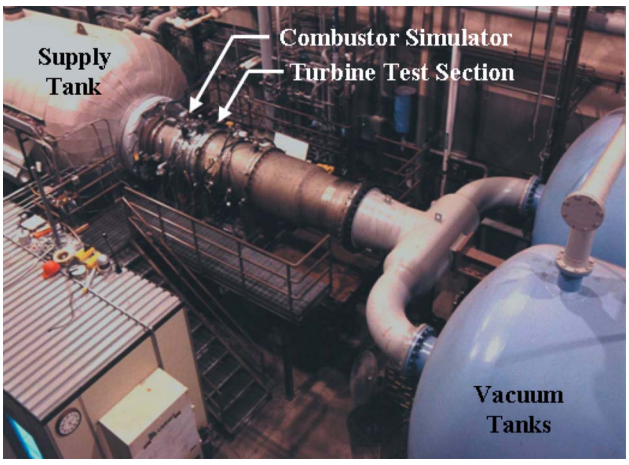

Fig. 2 Photograph of the TRF facility

Prior to testing, nitrogen gas was pressurized and heated within the supply tank, while the turbine section and vacuum tanks were evacuated. Testing began by activating the main valve located in the supply tank, at which time the gas flowed from the supply tank through the turbine test section and into the vacuum tanks. The mass flow rate was set by controlling the turbine pressure ratio using a variable area isolation valve that was located downstream of the main test section. The duration of a typical test was nominally 5 s. Due to the short test duration, all instrumentation measurements are recorded simultaneously in real time onto data storage units. The TRF facility was capable of simultaneously acquiring data across 200 12 bit channels with a maximum frequency response of 100 kHz and 200 16 bit channels with a maximum frequency response of 200 kHz. Signal conditioning on each channel took place using low pass filters and built-in amplifiers. All data reduction was performed at a later time.

The turbine inlet profile generator (combustor simulator) that was used in this study was designed and installed into the TRF facility to allow turbine testing to be performed with more realistic turbine inlet profiles of pressure, temperature, and turbulence intensity. Prior to installing the simulator, the temperature and pressure profiles at the inlet of the turbine section were nearly uniform in the radial and circumferential directions. The design of the simulator is documented in Barringer et al. [11]. The simulator essentially divides the supply tank flow into multiple concentric annular flow paths and directs each flow stream to a central annular chamber, similar to an actual aeroengine combustor. A magnified view of this central annular chamber is shown in Fig. 3 which highlights the general paths for the flow streams that inject flow into the chamber. These include the flow passing through the inlet, two rows of in-line opposed dilution holes (D_1 and D_2), and six staggered rows of film cooling (FC) holes. The influence of a

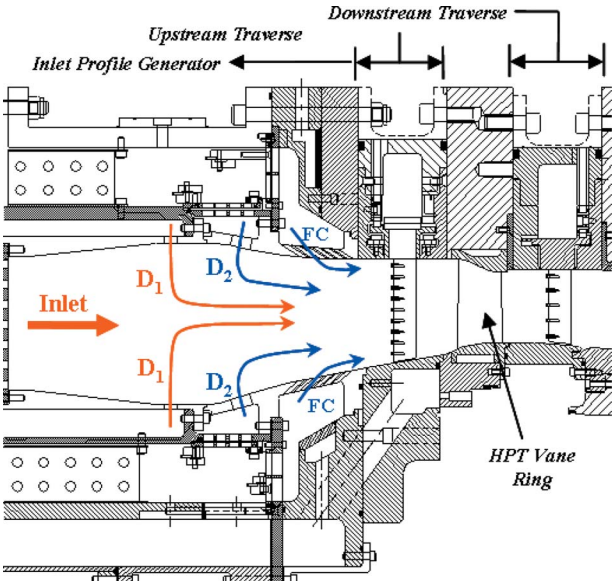

Fig. 3 Drawing of the combustor simulator central chamber indicating the general flow paths

particular flow stream over the turbine inlet profile can extend over a large radial range or it can be concentrated to a small local region. The effects of the film cooling flow were found to be evident in radial regions near the ID endwall at $0.0<Z/S<0.2$ and near the OD endwall at $0.8<Z/S<1.0$. The effect of the inlet core flow and dilution flows were found to be present over a larger span region of $0.2<Z/S<0.8$.

The turbine inlet and exit conditions were measured using multiple instrumentation rakes located on traverse rings upstream and downstream of the turbine section. The rakes, shown in Fig. 4, contained multiple thermocouples or multiple pressure transducers that were spaced to obtain measurements over equal annular flow areas. Most of the tests discussed in this study involved circumferentially traversing these rakes by approximately 90 deg during the blowdown to obtain both radial and circumferential profiles. However a few tests were performed in which the rakes were traversed by only 32 deg to allow a larger number of data points to be taken across multiple vane pitches. For the turbine inlet profiles being analyzed in the current study, a temperature rake containing seven 0.0254 mm diameter thermocouple beads with a thermal time constant of approximately 1.1 ms was used. Two pressure rakes were also used, each containing nine pressure

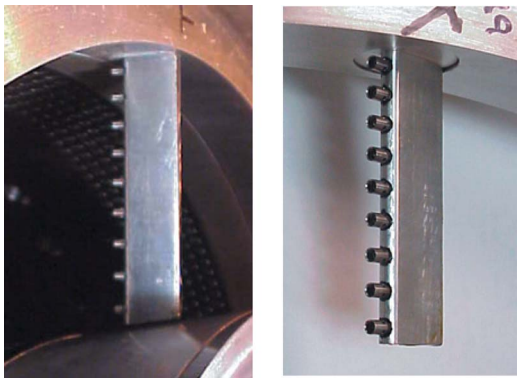

Fig. 4 Instrumentation rakes mounted in the upstream (left) and downstream (right) traverses

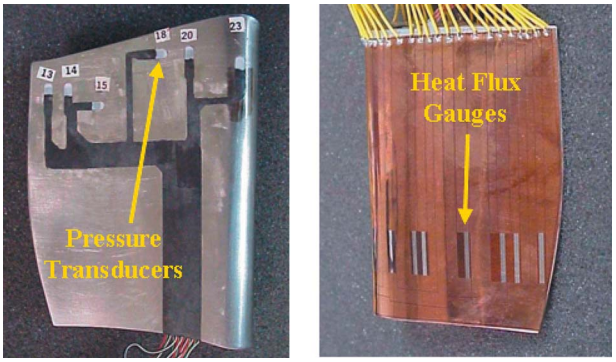

Fig. 5 Photographs of TRF vanes that were instrumented with pressure gauges (left) and HFGs (right)

transducers. Note that no boundary layer measurements were taken as these probes were fixed radially. All flow measurements were sampled at 20 kHz.

The pressure along the surface of several uncooled turbine vanes was measured using the 700 kPa miniature Kulite pressure transducers shown in Fig. 5. The transducers were mounted flushed with the vane surface along both the suction and pressure surfaces. Two vane span locations were selected for making surface pressure measurements including $Z/\mathrm{Sp}=0.5$ near midspan and $Z/\mathrm{Sp}=0.9$ near the OD. The Kulite transducers were also used to take static pressure measurements on the ID and OD endwalls at the vane inlet and exit. The total uncertainty associated with these measured pressures is at most 0.40% full scale.

The heat flux along the pressure and suction surfaces of several uncooled vanes was measured using thin film Oxford heat flux gauges (HFGs) [12] that are also shown in Fig. 5. Three span locations were selected for taking surface heat flux measurements including $Z/\mathrm{Sp}=0.24$ near the ID, $Z/\mathrm{Sp}=0.60$ near midspan, and $Z/\mathrm{Sp}=0.90$ near the OD. The gauges at $Z/\mathrm{Sp}=0.24$ and 0.60 had a spanwise extent of $\Delta Z/\mathrm{Sp}=0.15$, while the spanwise extent of the gauges at $Z/\mathrm{Sp}=0.90$ was $\Delta Z/\mathrm{Sp}=0.03$. Thermocouple beads with a diameter of 0.0254 mm were embedded into the vane metal directly beneath each HFG such that the beads were flushed with the vane surface.

By utilizing a semi-infinite solid analysis, the heat flux to the vane surface was calculated. The convection heat transfer coefficient, h, was then determined by dividing the local measured heat flux by the driving temperature. The driving temperature associated with the local heat flux was defined as the difference between the local vane surface temperature, T_w, and the adiabatic wall temperature, T_{aw}, in the vicinity of the gauge. The adiabatic wall temperature was calculated using the recovery factor and was based on the flow total temperature at the vane inlet at the same span location as the gauge. Typical values for this driving temperature difference were approximately 50–60 K. This driving temperature was then used to determine the local convection heat transfer coefficient on the vane surface. With h known, the length scale chosen for the Nusselt number was the vane axial chord length. The local Nusselt number was then obtained with the gas properties as taken from the local film temperature. This temperature was defined as the linear mean of the local vane surface temperature and the total temperature of the flow at the vane inlet at the same span location as the gauge.

Based on the uncertainties in the measurement of the HFG resistance and the uncertainty in calibration from resistance to temperature, the surface temperature uncertainty for the heat flux measurement was calculated to be +/−0.8 K for the HFGs. A jitter analysis described by Moffat [13] was then performed through the reduction scheme to obtain the uncertainty in the surface heat flux. This resulted in uncertainties in heat flux between 700 $\mathrm{W/m^2}$ and 2000 $\mathrm{W/m^2}$ depending on the gauge. The heat transfer coefficient

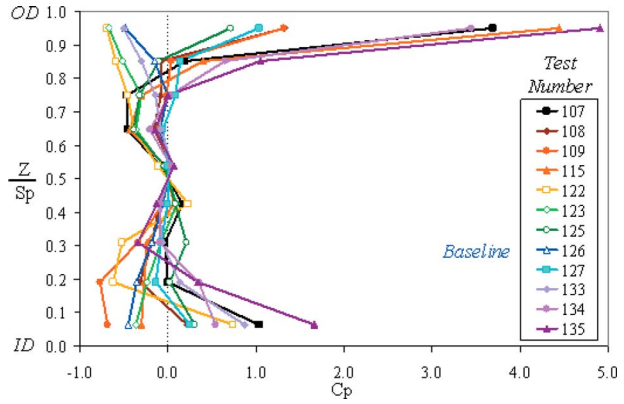

Fig. 6 Plot of several radial pressure profiles at the turbine vane inlet

uncertainty was determined to be about 30 $W/m^2 K$ for the thin film gauges based on an uncertainty in flow temperature of 0.7 K along with the hysterises in the measurement. This resulted in Nusselt number uncertainties between 5% and 9% depending on the location. The repeatability of these runs had a similar variation of 8–10%.

Test Conditions

The turbine inlet profiles that were analyzed for this study were generated during a series of benchmark tests to verify that the inlet profile generator operated as desired. The flow conditions corresponding to the verification tests are presented in Barringer et al. [1], which documents the overall operating range of the turbine inlet profile generator. The mean flow conditions at the turbine inlet for all of the profiles presented in this study correspond to $Re=2.1\times10^5$ and a Mach number of 0.1. The turbulence intensity associated with these turbine inlet profiles was also documented during the verification tests and was found to be in an elevated range between 20% and 30%, while the length scales were found to be between 1.5 cm and 1.9 cm. The longitudinal integral length scales were determined to be approximately 30% of the vane pitch or 2.3 times the vane leading edge diameter.

To document the effects of different turbine inlet profiles on turbine vane aerodynamics and heat transfer, a baseline test case was selected to make comparisons. The baseline that was chosen is test 126, which is characterized by both a relatively uniform radial pressure profile and a relatively uniform radial temperature profile. The turbulence intensity of the flow entering the turbine vane near midspan was at an elevated level near 21% for the baseline test 126. Comparisons of heat transfer and pressure loading are reported relative to those measured for the baseline case. The maximum percent deviations above and below the baseline results are also reported.

Aerodynamic Measurements at Midspan and in the Outer Diameter Region

Several radial pressure profiles at the turbine vane inlet are shown in Fig. 6. The profiles are plotted in terms of a normalized total pressure coefficient Cp defined as the local total pressure subtracted by the midspan total pressure all divided by the average dynamic pressure at the vane inlet. Note that by this definition Cp=0 at midspan. These radial profiles have been circumferentially (spatially) averaged across one full vane pitch along lines of constant radius that are spaced at equal annular flow areas and represent the mean vane inlet conditions. As shown in a previous investigation [1] there is about a 1% variation in the pressure and temperature profiles in the pitch variation, so essentially these profiles are circumferentially uniform.

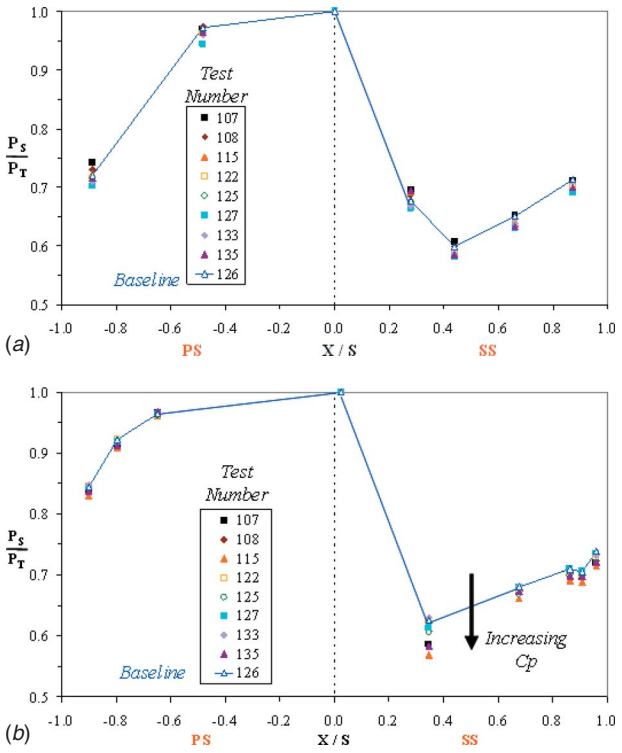

Fig. 7 Plot of the vane surface pressure at (*a*) *Z*/Sp=0.50 and (*b*) *Z*/Sp=0.90

A wide variety of radial profile shapes can be seen, including some that contain sharp gradients near the ID and OD endwalls. These gradients were the result of varying the amount of upstream film coolant being injected into the mainstream flow along the endwalls. As discussed in the previous paper [1], real engines exhibit Cp's in the range of $-0.5<Cp<2.0$, and this investigation covers a range somewhat larger than that. The peak Cp value near the ID and OD endwalls was found previously [1] to be directly related to the film cooling momentum flux ratio where an increase in this ratio resulted in an increase in the peak Cp value. It does have to be noted that the exact location and peak value of Cp is unknown as the rakes represent only specific discrete points. However, as discussed in a previous work [1], real engines exhibit Cp's in the range of $0.5<Cp<2.0$, so this investigation clearly covers that range and furthermore gives the designer some insight into whether any benefit could be obtained from utilizing even a larger range. It is also important to note that a negative Cp value does not indicate that the flow is in the reverse (upstream) direction; it simply means that the local total pressure is less than that at the midspan. This behavior can be seen for the baseline test 126 that possesses slightly less total pressure near the ID and OD endwalls (compared to the midspan) due to an absence of film coolant along the ID and OD endwalls for this particular test.

The corresponding pressure along the surface of the turbine vanes for these radial inlet pressure profiles is plotted in Fig. 7 at $Z/Sp=0.50$ and $Z/Sp=0.90$. Surface pressure measurements were not taken in the near ID endwall region. The ratio of the local vane surface static pressure, P_S, to the total pressure of the flow at the vane inlet, P_T, is plotted versus the vane surface distance, X/S, along both the SS and PS. Note that the normalizing total pressure, P_T, used in Fig. 7 is the surface pressure measured at the leading edge of the vane at $X/S=0.0$ at the same corresponding span location. In Fig. 7 it can be seen that the effect of the surface pressure loading due to the inlet pressure profiles was less significant at the midspan than at the OD region location at $Z/Sp=0.90$. This was due in part to small changes in the midspan Cp for these cases, coupled with the fact that the vane geometry in the

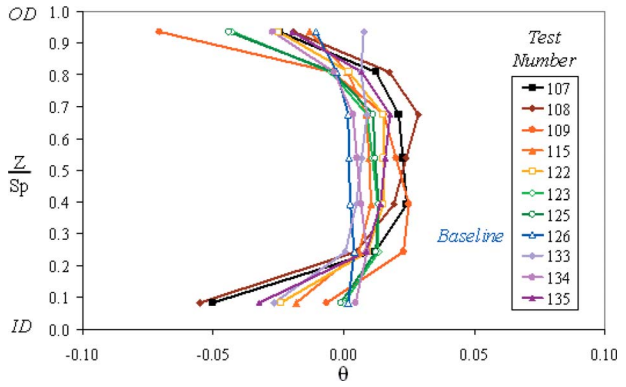

Fig. 8 Plot of several radial temperature profiles at the turbine vane inlet

midspan region is nearly two dimensional. Therefore limited secondary flow changes are expected at midspan. The maximum percent deviation of P_S/P_T from the baseline test that was observed at $Z/Sp=0.50$ was approximately 3.0% for test 107, which occurred on the PS of the vane near the trailing edge at $X/S=-0.89$.

More significant differences occur at $Z/Sp=0.90$. The data on the vane SS indicate that the different inlet pressure profiles had a significant impact on the surface pressure from $X/S=0.35$ to the trailing edge. Figure 7(*b*) indicates that the most significant effect of the different inlet pressure profiles occurs on the vane suction surface near $X/S=0.35$, which is close to the minimum passage area for this vane geometry. At this location, test 115 (containing a large Cp peak value near 4.5) resulted in a maximum P_S/P_T deviation of 9.1% below the baseline test (over three times the maximum at midspan), and test 133 (containing a negative Cp peak value near −0.5) resulted in a maximum deviation of 0.7% above the baseline test. These two tests resulted in a P_S/P_T pressure ratio range of approximately 9.8% at this X/S surface location, thus illustrating that the local aerodynamic loading of the vane can change as much as 10% depending on the inlet total pressure profile.

At 90% span, Fig. 7(*b*) also shows that the percent deviation from the baseline test was relatively small on the PS of the vane (similar to most locations on the PS at midspan). In general, an increase in the pressure profile Cp peak along the endwall resulted in a decrease in the ratio of P_S/P_T. These results indicate that higher momentum fluid along the OD endwall results in an increase in the aerodynamic loading of the vane at this span. It is believed that the secondary flows are moving lower pressure fluid from the lower span into this region on the SS consistent with the work of Colban et al. [8]. One additional comment is that the total pressure at the 90% span stagnation location, used as the reference for determining the loading, is at a lower level than midspan, giving rise to a higher loaded airfoil.

Heat Transfer Measurements in the Inner and Outer Diameter Regions

Several different radial temperature profiles at the turbine vane inlet are shown in Fig. 8. The profiles are plotted in terms of a nondimensional temperature coefficient θ defined as the local total temperature subtracted by the average total temperature entering the turbine, all divided by the same average temperature. These radial profiles have been circumferentially averaged across one full vane pitch along lines of constant radius that are spaced at equal annular flow areas. The average temperature at the simulator exit was determined by integrating the spanwise profile from the seven headed rake from hub to tip. To obtain a better approximation of this average temperature, the temperature data were extrapolated to the endwalls using a constant slope between the outermost and second outermost data points. The actual average temperature varied for each test but was in the range of 380–435 K.

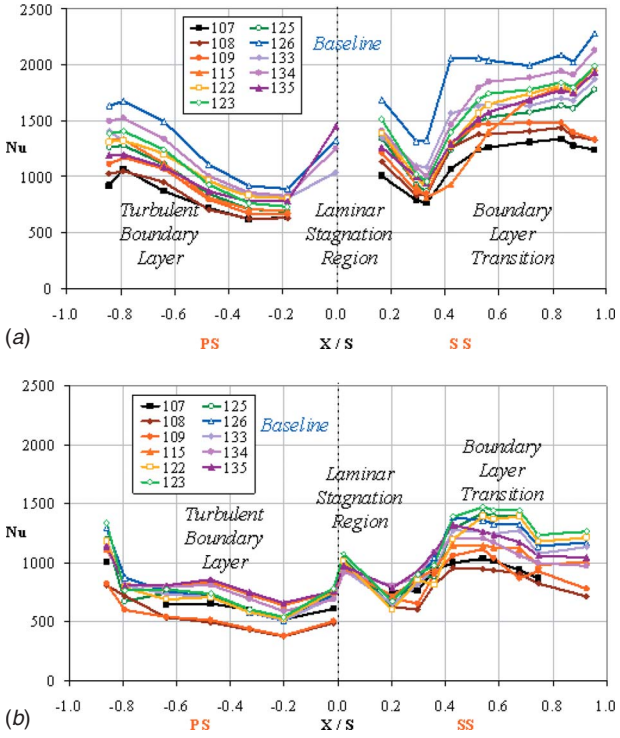

Fig. 9 Nusselt number distribution along the vane surface in the ID region at (*a*) *Z*/Sp=0.24 and in the OD region at (*b*) *Z*/Sp=0.90

The inlet temperature profiles include some that contain considerable gradients along the endwalls (tests 107 and 108) and some that are nearly uniform over the entire span (baseline case test 126). Figure 8 shows that the most significant differences occur in the two span regions $0<Z/Sp<0.25$ and $0.75<Z/Sp<1.0$. Again this was attributed to the varying amounts of upstream film coolant being injected along the ID and OD endwalls at different momentum flux ratios and different temperatures relative to the core flow. The midspan region indicates more uniform temperature distributions compared to the ID and OD regions, with the variations resulting from differing upstream dilution flow injections. The shape of the profiles are consistent with engine combustor profiles, as discussed in an earlier work [1], with the overall minimum to maximum magnitude variation in θ being slightly less in this investigation than in the engine.

The corresponding heat transfer distribution along the vane surface for the different inlet temperature profiles is shown in Fig. 9 in terms of the Nusselt number, which is a dimensionless temperature gradient at the wall surface. The Nu distributions near the ID at $Z/Sp=0.24$ are shown in Fig. 9(*a*), while Fig. 9(*b*) shows the Nu heat transfer distributions near the OD at $Z/Sp=0.90$. The results in the ID and OD regions only are presented to focus on the locations where the heat transfer was significantly altered as Fig. 9 shows. The midspan gauges showed similar trends as seen at 24%. It can also be seen in Fig. 9 that the overall heat transfer variations and levels are higher at $Z/Sp=0.24$ compared to $Z/Sp=0.90$. This can be explained in part by recognizing that the HFGs located at the $Z/Sp=0.24$ span position extend from approximately $Z/Sp=0.20$ to 0.35, and therefore their measurements were influenced by the higher turbulent flow that dominates the midspan region. In addition the location of the passage vortex exiting the vane row could be contributing to the higher levels. For all of the tests, the Nu distributions showed elevated levels

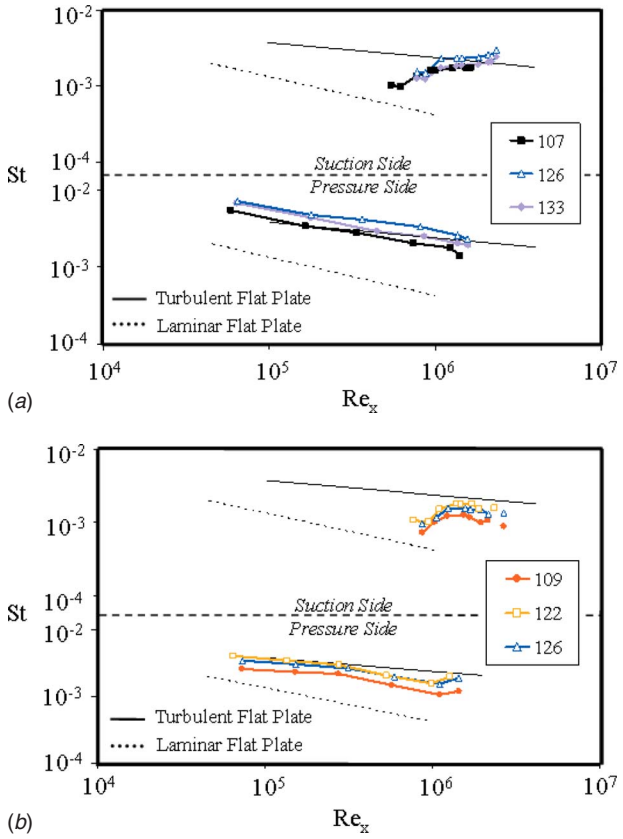

Fig. 10 Plot of the Stanton number versus Reynolds number along the vane surface at (*a*) *Z*/Sp=0.24 and (*b*) *Z*/Sp=0.90

near the leading edge stagnation region where the flow was within the laminar flow regime. The Nu levels then decreased with increasing distance from the leading edge on both the pressure and suction surfaces. It is evident from Fig. 9 that transition to a turbulent boundary layer begins on the suction surface near $X/S=0.3$ at both span locations. This transition region extended over the majority of the suction surface toward the trailing edge. The Nu distribution on the PS of the vane from $X/S=-0.3$ to the trailing edge was indicative of a turbulent boundary layer.

The heat transfer along the surface of the vane for the baseline test 126 is also illustrated in Fig. 10 in the form of Stanton number versus Reynolds number based on surface distance from the leading edge, Re_x. The data in Fig. 10 correspond to PS gauges between $-1.0<X/S<-0.2$ and SS gauges at $0.3<X/S<1.0$. The vane leading edge region data were not included in the figure. The velocity scale used for both the Stanton and Reynolds numbers was the *local* freestream velocity. For the 24% gauges the Mach number at 50% span was used to aid this calculation as the Mach number at 24% span was unknown. The thermodynamic fluid properties were evaluated at the local film temperature. Data are plotted for both span locations at $Z/Sp=0.24$ and 0.90 and both the PS and SS of the vane. Also plotted in this figure are the Stanton number correlations for laminar and turbulent flows over a flat plate. Figure 10(*a*) compares the baseline test results to the heat transfer results from tests 107 and 133, which were selected to illustrate the full St range of the data at $Z/Sp=0.24$. Figure 10(*b*) compares the baseline test results to the heat transfer results from tests 109 and 122, which were also selected to illustrate the full Stanton number range of the data at $Z/Sp=0.90$.

The results shown in Fig. 10 are important for two reasons. First, they show that on the PS the Stanton numbers follow the general slope of the turbulent correlation. Therefore, although the levels of heat transfer differ at the two spans, both pressure surfaces are fully turbulent. Second, they show that on the SS the Stanton numbers appear to make a transition from a laminar behavior to a turbulent behavior, and this agrees with the Nu distribution for the SS.

The overall variation in Nu from test to test is considerable at both span locations and was attributed to the different vane inlet profiles effect. This will be discussed more in the next section. Near the ID, at $Z/Sp=0.24$, it can be seen that the Nu distribution along the vane surface for the baseline case is consistently higher than the other test cases on both the pressure and suction surfaces. It was found that at this span location the different inlet profiles reduced the baseline heat transfer by 30–40% over the majority of the vane surface with a maximum reduction of 48% for test 107, which has a Cp=1.0 and a $\theta=-0.05$. At 90% span, it was found that certain inlet profiles could increase the baseline heat transfer by 10–20% over the majority of the vane surface, for example, test 122 which has a Cp=0.75 and $\theta=-0.002$. While other inlet profiles resulted in a decrease in the baseline heat transfer by 25–35% over the majority of the vane surface, for example, test 109 which also has a Cp=1.0 and a $\theta=-0.007$ but on the OD side.

Influence of Inlet Profiles

Returning to the results shown in Fig. 9(*a*), an investigation was performed into the effects on the vane heat transfer due to temperature profiles shown in Fig. 8. As the temperature profile shifts from a flat profile like the baseline test 126 to a slightly shaped profile like test 123, to a higher gradient profile like test 122, to the largest gradient shape tested like test 108, the Nusselt number clearly decreases across the majority of the airfoil. Creating the greatest thermal profile is clearly beneficial in reducing the heat transfer for this span. This phenomenon occurred on both surfaces, leaving the baseline test (126) as the highest heat loaded case.

The isolated effect of the turbine inlet pressure profile on the vane surface heat transfer was determined by comparing the Nusselt number curves in Fig. 9 for tests having similar inlet *temperature* profiles but different inlet *pressure* profiles. For example, in the ID region near $Z/Sp=0.24$, Fig. 8 shows that tests 126 and 134 had very similar inlet temperature profiles that possessed moderate gradients near the endwalls, but Fig. 6 shows that these same two tests had inlet pressure profiles with different positive Cp peak values. In Fig. 9(*a*) it can be seen that test 135 (with a higher Cp) resulted in lower Nusselt numbers at this span location. A similar result was also found when comparing test 123 to 125, test 122 to 135, and also test 108 to 107. This led to an important conclusion that at $Z/Sp=0.24$ the test possessing a larger peak Cp value near the ID endwall resulted in lower Nusselt numbers for tests with similar inlet temperature profiles. This decrease was readily apparent along the entire PS. It also occurred on the SS but was most prevalent aft of $X/S>0.4$.

This observation is consistent with previous findings in the literature. For example, it was found within the work of Hermanson and Thole [8] and Colban et al. [9] that the turbine vane inlet pressure profile near the endwall directly affects the development of the secondary flows that exist within the turbine vane passage. The secondary flow vectors shown in Fig. 1 dictate the heat transfer along the vane surface and endwall region. The forward facing peak in the radial inlet pressure profile produced two vortices as the flow approaches and reached the leading edge of the vane. The span location that separated these two vortices was dictated by the span location of the Cp peak in the inlet pressure profile. It is believed that the relative size and strength of these two vortices directly depend on both the peak Cp value and the spanwise thickness of the forward facing region of the pressure profile. For this set of experiments it was not possible to determine the exact location of the peak in the spanwise total pressure at the inlet, but it is believed to be less than 10% span from either endwall due in part to the results of the computational fluid dynamics (CFD) work documented in Kunze et al. [14]. Due to the fact that the ID

and OD endwalls possess different contraction geometries, the secondary flow development will be slightly different on the ID versus the OD. However it was the overall flow changes with respect to a typical boundary layer behavior that was significant.

For a test case without utilizing the simulator film coolant jets along the endwall, like the baseline test 126, the turbine vane inlet pressure profile took the shape of a standard turbulent boundary layer profile (type A). In Fig. 1 it can be seen that the passage vortex for these inlet pressure profiles would have a slight impact on the flowfield at the $Z/\mathrm{Sp}=0.24$ span location. Therefore, the heat transfer measurements taken at this span were only slightly impacted by the passage vortex structure and therefore the dominant driver for heat transfer was the temperature found at about 24% span. However for a test similar to 134 that had a similar temperature profile (as shown in Fig. 8) but a significant peak in the pressure profile (type B), the existence of the counter-rotating vortex will directly impact the development of the passage vortex, for example, by confining it to a span region closer to the endwall or by reducing its vorticity, as seen in Fig. 1. This change in flow structure will have a definitive change in the heat transfer at 24% span as indicated in the reduction of the Nusselt number shown in Fig. 9(*a*).

Focusing next on the OD region, examining the temperature and pressure profiles at 90% span helps to understand why the Nusselt number increased in some cases and decreased in others. On the SS, the cases with higher Nusselt numbers than the baseline case were those that have negative Cp values near the OD endwall. Again this does not imply that an inlet profile that has a higher midspan total pressure causes a reverse flow at the endwall. However it infers that this condition would result in a more typical turbulent boundary layer. What these results suggest is that to keep the Nusselt numbers relatively low near the endwall, some high total pressure fluid is desirable to buffer the hot flow away from the endwall to avoid this increase in heat transfer. In practice, the cases with negative Cp result in strong type A profiles. These cases thereby generated a larger and stronger passage vortex, as indicated in Fig. 1, and thus increased the 90% heat transfer levels particularly aft of $X/S>0.4$, as shown in Fig. 9(*b*). By increasing the near wall Cp, the passage vortex is broken up somewhat and the hottest midspan gases were not able to reach the endwall region.

On the PS, the low Cp cases also resulted in elevated PS Nusselt numbers but are joined by the very high Cp cases (tests 135, 107, and 134). These latter cases correspond to the type B inlet pressure profiles, but due to the very high Cp values, they resulted in the formation of a stronger passage vortex and a larger counter-rotating vortex system. It is believed that these two vortices caused the elevated heat transfer in the 90% region particularly on the PS. This is further enhanced by the stagnation region in between the vortices, as indicated in Fig. 1. While the exact location of the stagnation line was unknown, it can be expected that the strength of the vortices (as well as the size of the stagnation region) would increase with increasing Cp values and thus heat transfer.

The position of these vortices helps to explain some of the differences in trends between the 90% and 24% span locations. While at 24%, the higher Cp peaked pressure profile resulted in the lower Nu, this trend did not hold true at the 90% span. Clearly the highest Cp profiles caused an increase in the heat transfer, which suggests that there may be an optimum profile. In Fig. 9(*b*), test 108 displayed the lowest Nusselt number along the entire vane surface at 90%. This run was characterized by having a temperature profile with large radial gradients, which was previously shown to benefit the heat transfer at 24% as well. It furthermore has a high, but not extremely high, Cp value along the OD endwall. Its value is closer to 1.0, and while there are not enough runs within this Cp range to determine the exact optimum, clearly increasing the value to a Cp of 3.0 (test 107) is detrimental. This was also consistent with the results at the 24% span as the ID Cp profiles were all less than 2.0. So for the ID profiles, increasing the Cp was still a benefit as they did not reach this "peak" benefit value. Since tests at higher Cp were not run on the ID, it is uncertain if these Nu levels would subsequently decrease, but it is believed that they would.

Table 1 Range of span locations that influence the driving temperature at $Z/\mathrm{Sp}=0.24$ and $Z/\mathrm{Sp}=90$

	Range of span locations (%)			
Side of vane	Suction side		Pressure side	
Profile type	A	B	A	B
24% Span	24	24–35	24	10–24
90% Span	90–100	85–90	85–90	90–95

As the pressure profile increases from a case like test 122 toward test 126, the strength of the passage vortex decreases. Clearly there is some condition where the strength of this vortex will be near zero. This would be the ideal condition for reducing the secondary flows but not necessarily for achieving the lowest Nu. As the Cp value continues to increase, the passage vortex will form again as a pressure gradient was established as the flow approached the wall. Now, however, at the spanwise position of the peak Cp value, an inflection point was created, serving to swirl the rest of the flow back toward midspan. This served to circulate the hot flow away from the endwall, keeping the endwall cooler. As shown in Fig. 1, between these two vortices there was also a stagnation region formed, which served to increase the heat transfer in this region. At the highest Cp, this stagnation region can be expected to be large, elevating the local heat transfer. Likewise the strength of the two vortices would be expected to increase, further enhancing the Nusselt number.

Influence of Driving Temperature

Utilizing the velocity vector trends shown in Fig. 1 and keeping in mind that the inflection points for the inlet profiles examined in this study are believed to be slightly closer to the endwall, a range of span locations that influence the local driving temperature was developed in Table 1. This table was built by determining where the secondary flow circulation patterns would bring the flow based on the velocity vector distribution shown in Fig. 1. It is understood that the values given in Table 1 are not exact, but they can be used as a general method to help determine how significant the impact of driving temperature is for the predicted Nusselt numbers. For example, for a type A profile at 24% there was relatively minimal secondary flow so the inlet profile at 24% would continue through the vane uninterrupted. The single point values indicate that a span range to average over was unnecessary, and the inlet total temperature at that same span location may be used as a good indicator of the true driving temperature. However at the 90% span Fig. 1 indicates a vortex with size in the 85–100% span moving fluid down the SS and up the PS of the airfoil.

For nonuniform vane inlet temperature profiles, a relatively warmer or cooler flow circulated from one span location to another span location changes the value of the driving temperature that should be used to determine the local values of h and Nu. The method of determining this driving temperature discussed in Povey et al. [5] could not be used in the current study since the technique assumed that the convection heat transfer coefficient was unchanged with and without vane inlet temperature distortion. In the current study, the inlet total pressure profiles vary significantly from one test to the next. This variation affects the secondary flow patterns within the vane passage and therefore also changes the local convection heat transfer coefficient from test to test.

To illustrate the effect of the secondary flow circulation patterns on the driving temperature, the Nusselt number distributions at both span locations are plotted in Fig. 11 for a test with a type A

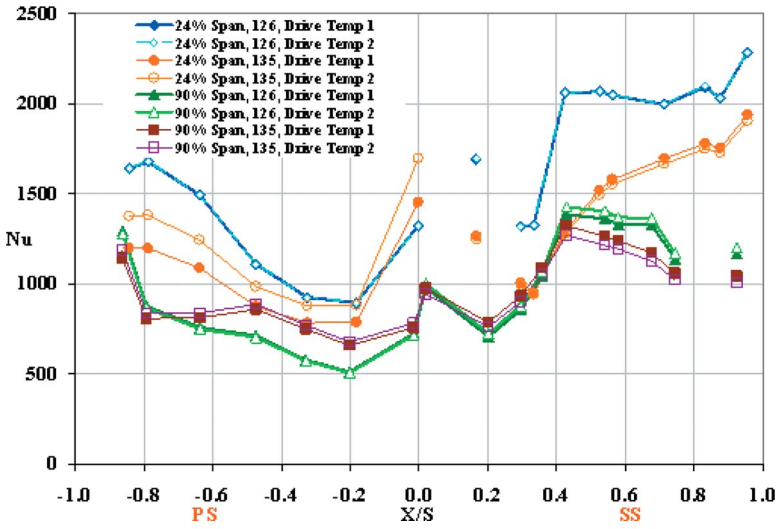

Fig. 11 Plot showing the effect of driving temperature on Nusselt number at the *Z*/Sp=0.24 and *Z*/Sp=0.90 measurement locations for a vane inlet pressure profile corresponding to type A (test 126) and type B (test 135)

inlet pressure profile (Test 126) and a type B inlet pressure profile (test 135). The Nusselt number distribution is plotted for two different driving temperatures. The first driving temperature, designated as "Drive Temp 1," is the original driving temperature defined in the nomenclature and used in Fig. 9. The second driving temperature, designated as "Drive Temp 2," is also the original driving temperature definition but utilizes T_{aw} based on the mean flow temperature within the vane span range described in Table 1.

Figure 11 shows this comparison for the baseline test 126, which had nearly uniform inlet profiles of both pressure and temperature. As expected for a case where the vane inlet flow temperature does not vary significantly in the span direction, the change in driving temperature was small and the impact on the predicted Nusselt number was also small at both span locations. However, the combination of a significant pressure profile causing more secondary flow circulation coupled with a significant thermal gradient in the temperature profile will affect the true driving temperature. Figure 11 also shows this comparison for test 135, which exhibited these types of profiles. The effect of the two different driving temperatures on Nu for test 135 was noticeable over the majority of the vane surface at both span locations. At $Z/\mathrm{Sp}=0.90$ these changes were on average near −4% on the SS and +4% on the PS. At $Z/\mathrm{Sp}=0.24$ the changes in Nu were on average near −2% on the SS and +12% on the PS. This indicates that the SS Nusselt number would have been overpredicted by approximately 3% had the more correct driving temperature not been taken into account, and the PS Nu was substantially underpredicted without accounting for the secondary flow effects.

Conclusions

Several different temperature and pressure radial profiles representative of those exiting aeroengine combustors were investigated to determine their effects on high pressure turbine vane heat transfer and aerodynamic loading. The profiles were generated using a turbine inlet profile generator located in the TRF at the AFRL. Surface pressure measurements were analyzed at two span locations including midspan at $Z/\mathrm{Sp}=0.50$ and near the OD at $Z/\mathrm{Sp}=0.90$. Heat flux measurements were analyzed near the ID and OD endwalls at $Z/\mathrm{Sp}=0.24$ and 0.90.

The surface pressure measurements showed that increasing the Cp at the inlet to 4.5 increased the baseline aerodynamic loading as much as 9% near the OD endwall. This percentage was defined as the local deviation of the quantity P_S/P_T from the baseline test, which was characterized by a nearly uniform inlet pressure. These same profiles had far less effect at midspan, only resulting in increases of 3%. The different inlet temperature and pressure profiles altered the vane surface heat transfer significantly along both the PS and SS of the vanes. Near the ID endwall at $Z/\mathrm{Sp}=0.24$, increasing the Cp of the inlet profile reduced the baseline heat transfer up to 30–40% over the majority of the vane surface. Near the OD endwall, at $Z/\mathrm{Sp}=0.90$, it was found that negative Cp inlet profiles could increase the baseline heat transfer by 10–20% over the majority of the vane surface, while profiles with moderate Cp values of around 1.0 resulted in a decrease in the baseline heat transfer by 25–35%. The isolated effect of the inlet pressure profile on vane heat transfer showed that the pressure profile plays an important role in the vane heat transfer. In general, an increase in the pressure profile Cp peak value for similar inlet temperature profiles leads to a reduction in the Nusselt number distribution over large portions of the pressure and suction surfaces of the vanes up to some optimum value. It is suggested that there is an ideal pressure profile somewhere around a Cp of 1.0 for reducing the secondary flows and thus the heat load to the turbine. It is also suggested that the temperature profile with the largest radial gradients provides the greatest heat transfer benefit.

The authors recommend that traditional models of passage vortex evolution developed for typical boundary layer profiles (type A) should not be applied for turbine vane inlet flows that contain forward facing pressure regions with inflection points near the endwalls (type B profiles). The heat transfer within the vane passage will be significantly different between type A and B inlet profiles due to the different secondary flow development, vortex strength, and vortex size within the passage.

The vane inlet pressure profile near the endwalls will directly influence the secondary flow circulation patterns that exist within the vane passage. The size and strength of the vortices within the passage will dictate the thermal migration in the spanwise direction, which will in turn affect the heat transfer driving temperature at the surface of the vanes and endwalls. This paper provided a description of this thermal migration process for different inlet pressure profile types and showed that very close attention must be paid to the driving temperature being used when predicting the Nusselt number distribution along the vane surface and endwalls. Otherwise, turbines operating with inlet profiles similar to those considered in this study could be exposed to local heat transfer significantly different from that intended or expected.

Acknowledgment

The authors would like to thank Michael Kobelak, Terry Gillaugh, and Dr. Douglas Rabe from the AFRL/PRTE Technology Evaluation Branch for their guidance and help in conducting these experiments and to Robert Free for the installation of the HFGs on the vanes as well as for the manufacture of the rakes. The authors would also like to thank the Air Force Research Laboratory at Wright Patterson Air Force Base for funding and sponsoring this research effort.

Nomenclature

C = vane axial chord length
Cp = pressure coefficient, $\mathrm{Cp}=(P_t-P_{t_{\mathrm{ms}}})/1/2\rho_{\mathrm{av}}U_{\mathrm{av}}^2$
d = hole diameter
h = convection heat transfer coefficient, $h=q''/(T_{\mathrm{aw}}-T_w)$
Nu = Nusselt Number, $\mathrm{Nu}=h_{\mathrm{local}}C/k_f$
P = pressure or vane pitch
PS = pressure side
q'' = heat flux
Re = Reynolds number, $\mathrm{Re}=U_{\mathrm{av}}C/\upsilon_{\mathrm{av}}$
S = total vane surface length
Sp = vane span
SS = suction side
St = Stanton number, $\mathrm{St}=h_{\mathrm{local}}/(\rho_f C_p U_{\mathrm{local}})$
T = temperature
U = velocity
X = axial direction or surface distance
Y = pitch direction
Z = span direction

Greek

ν = kinematic viscosity
ρ = density
θ = nondimensional temperature, $\theta=(T-T_{\mathrm{av}})/T_{\mathrm{av}}$

Subscripts

av = mean or average conditions
aw = adiabatic wall
f = film conditions
FC = film cooling
MS = midspan
S = flow static conditions
T = flow total conditions
w = vane wall surface
x = surface distance along vane

References

[1] Barringer, M., Thole, K., and Polanka, M., 2007, "Experimental Evaluation of an Inlet Profile Generator for High Pressure Turbine Tests," ASME J. Turbomach., **129**, pp. 382–393.
[2] Cattafesta, L., 1988, "An Experimental Investigation of the Effects of Inlet Radial Temperature Profiles on the Aerodynamic Performance of a Transonic Turbine Stage," MS thesis, MIT.
[3] Shang, T., Guenette, G., Epstein, A., and Saxer, A., 1995, "The Influence of Inlet Temperature Distortion on Rotor Heat Transfer in a Transonic Turbine," AIAA Paper No. 95-3042.
[4] Chana, K., Hurrion, J., and Jones, T., 2003, "The Design, Development and Testing of a Non-Uniform Inlet Temperature Generator for the QinetiQ Transient Turbine Research Facility," ASME Paper No. 2003-GT-38469.
[5] Povey, T., Chana, K., Jones, T., and Hurrion, J., 2005, "The Effect of Hot-Streaks on HP Vane Surface and Endwall Heat Transfer: An Experimental and Numerical Study," ASME Paper No. GT2005-69066.
[6] Krishnamoorthy, V., Pai, B., and Sukhatme, S., 1988, "Influence of Upstream Flow Conditions on the Heat Transfer to Nozzle Guide Vanes," ASME J. Turbomach., **110**, pp. 412–416.
[7] Van Fossen, J., and Bunker, R., 2002, "Augmentation of Stagnation Region Heat Transfer Due to Turbulence from an Advanced Dual-Annular Combustor," ASME Paper No. GT2002-30184.
[8] Hermanson, K., and Thole, K., 2000, "Effect of Inlet Conditions on Endwall Secondary Flows," J. Propul. Power, **16**(2), pp. 286–296.
[9] Colban, W., Thole, K., and Zess, G., 2002, "Combustor Turbine Interface Studies—Part 2: Flow and Thermal Field Measurements," ASME Paper No. 2002-GT-30527.
[10] Haldeman, C. W., Dunn, M. G., MacArthur, C. D., and Murawski, C. G., 1992, "The USAF Advanced Turbine Aerothermal Research Rig (ATARR)," *NATO AGARD Propulsion and Energetics Panel Conference Proceedings 527*, Antalya, Turkey.
[11] Barringer, M., Thole, K., and Polanka, M., 2004, "Developing a Combustor Simulator for Investigating High Pressure Turbine Aerodynamics and Heat Transfer," ASME Paper No. GT2004-53613.
[12] Jones, T. V., 1995, "The Thin Film Heat Transfer Gauge: A History and New Developments," Proc. Inst. Mech. Eng., Part C: J. Mech. Eng. Sci., **209**(C510), p. 150–160.
[13] Moffat, R. J., 1982, "Contributions to the Theory of a Single-Sample Uncertainty Analysis," ASME J. Fluids Eng., **107**, pp. 153–160.
[14] Kunze, V. R., Wolff, M., Barringer, M. D., Thole, K. A., and Polanka, M. D., 2006, "Numerical Insight Into Flow and Thermal Patterns Within an Inlet Profile Generator Comparing to Experimental Results," ASME Paper No. GT-2006-90276.